Design of a flexible end-effector based on characteristics of tomatoes

Kehong Zhou[1,2], Liru Xia[2], Jun Liu[2], Mingyan Qian[2], Jie Pi[2*]

(1. *Institute of Agricultural Engineering, Jiangsu University, Zhenjiang 212001, China*;
2. *Institute of Agricultural Facilities and Equipment, Jiangsu Academy of Agricultural Sciences, Key Laboratory of Protected Agriculture Engineering in the Middle and Lower Reaches of Yangtze River, Ministry of Agriculture and Rural Affaires, Nanjing 210014, China*)

Abstract: The end-effector is the last executing part of the interaction between robots and fruits. In this study, the physical characteristics of tomatoes and the tomato end-effector of the fluidic elastomer actuator type were studied. There was no correlation between the test point, the mass, the size and the rupture force of tomatoes. The non-destructive clamping force of tomatoes was 11.13 N. There were statistically significant correlations between the number of finger chambers, the transverse diameter of tomatoes, the inflation pressure and the clamping force. The inflation pressure and the size of tomatoes were directly proportional to the clamping force. Since fingers with more chambers had higher flexibility, the number of chambers was inversely proportional to the slope of the horizontal force-pressure curve, and the number of chambers was directly proportional to the angle between the total clamping force and the horizontal direction. A flexible end-effector was designed by genetic algorithm according to the physical characteristics of tomatoes and the simulation results of the finger of the end-effector. The test results of the end-effector showed that the tomatoes would be successfully clamped by the end-effector composed of three four-chamber fingers in a static situation with the inflation pressure less than the optimized inflation pressure (28.293 kPa). When in a dynamic situation, the success rate of tomatoes being clamped by the end-effector with an inflation pressure of 29 kPa was 97%. The tomatoes in the static clamping test and the dynamic clamping test were not damaged.

Keywords: end-effector, fluid elastomer actuator, non-destructive, flexible, genetic algorithm, characteristics of tomatoes
DOI: 10.25165/j.ijabe.20221502.6672

Citation: Zhou K H, Xia L R, Liu J, Qian M Y, Pi J. Design of a flexible end-effector based on characteristics of tomatoes. Int J Agric & Biol Eng, 2022; 15(2): 13–24.

1 Introduction

Originating in South America, tomatoes were introduced to Europe in the 16th century, and China in the 17th century[1]. Tomatoes, which have rich nutrition and unique flavors, are not only important model plants in the field of botany research, but also essential vegetables in people's daily diets[2-5]. Tomatoes in China is being cultivated on over 1.1 million hm^2 of land with an output of about 50 million t, and the output is showing a growth trend[6,7]. Picking and sorting fruits and vegetables are the most time-consuming and labor-intensive parts of the production process[8,9]. The research in the field of end-effector is of great significance to liberate labor, improve production efficiency, and reduce production costs[8,9].

In current studies, end-effectors for tomatoes were designed for the picking process. The end-effectors designed by Beijing Research Centre of Intelligent Equipment for Agriculture sucked tomatoes into the rotating tray and fixed tomatoes[10,11], which were difficult to apply to the post-processing of tomatoes. The end-effectors designed by the University of Tokyo[12] and Southwestern University[13] were rigid end-effectors, which had complex structure and low adaptability. Therefore, there was a lack of end-effectors for tomatoes' post-processing process. Flexible end-effectors, which are made of flexible material performing excellent in compliance and adaptability, are suitable for post-processing of tomatoes. Variable stiffness type, adhesion type, contact-driven deformation type and fluidic elastomer actuator type are the four types of end-effectors commonly used in clamping fruits and vegetables.

The end-effector with variable stiffness can wrap and fix the target[14-16]. Kansai University designed a vacuum end-effector imitating how the sucker of octopus work[17]. With such vacuum end-effector, objects were clamped by the end-effector by jamming transition. Such working principle is slow in response and not suitable for clamping fruits and vegetables.

The end-effector clamping by control adhesion is characterized by stability[18,19]. University of California San Diego designed a soft robotic end-effector with gecko-inspired adhesive[20]. During operation, large shear friction was generated by the end-effector to stabilize the clamping. However, tomato epidermis is fragile and can be easily damaged.

The contact-driven deformation end-effector is easy to fabricate[21-23]. Wageningen University and Research Centre designed an end-effector with fin-ray structure[24,25]. The end-effector bent when it touched the object and conformed to the surface shape of the object. Clamping was carried by the reaction force of flexible material. The agricultural R&D company Octinion in Belgium designed a strawberry picking robot whose end-effector was composed of two soft frame structures[26], by which the strawberries would be wrapped. The contact area between a strawberry and the soft frame structure was large and the pressure was uniform. Due to weak clamping force and unstable holding, the contact-driven deformation end-effector was unfeasible to be applied to tomato clamping.

Received date: 2021-04-13 **Accepted date:** 2021-08-28
Biographies: Kehong Zhou, research interests: agricultural harvesting and sorting robot, Email: zhoukh97@163.com; **Liru Xia,** Research Fellow, research interests: agricultural engineering, Email: xlrjaas@126.com; **Jun Liu,** research interests: intelligent sensor and robots, Email: nkyliu@163.com; **Mingyan Qian,** research interests: agricultural engineering, Email: nkyqian@163.com; **Jie Pi,** research interests: agricultural engineering, Email: pijiejaas@163.com.
***Corresponding author: Jie Pi,** research interests: agricultural engineering. Jiangsu Academy of Agricultural Sciences, Nanjing 210014, China. Tel: +86-25-84390965, Email: pijiejaas@163.com.

The fluidic elastomer actuator with geometric asymmetry or material anisotropy is capable of transforming the cavity expansion into a bending of the whole actuator[27]. The end-effector designed by Northeastern University was a fluidic elastomer actuator[28]. While with multiple sensors installed inside, the cost of the end-effector was largely increased. Nanjing Agricultural University designed an end-effector for mushroom[29]. Such end-effector was designed to produce clamping force in a horizontal way as mushrooms can only be clamped from their pilei and share similar sizes, ranging from 8 to 10 mm. Since tomatoes can be clamped from more parts and sizes of tomatoes can be quite different (60-90 mm), it is unreasonable to design the end-effector for clamping tomatoes by adopting the design principle for mushrooms.

In this study, a flexible end-effector based on tomato characteristics was designed to be applied to the post-processing of tomatoes. The bending performance of the finger and the clamping performance of the end-effector in different situations were discussed in this paper. This study could provide valuable references for optimizing agricultural end-effector.

2 Physical characteristic test

The geometric sizes and mass, the static friction, the compression characteristics, and the damage characteristics of tomatoes were studied to design tomato end-effector. The tested samples were mature Momotaro tomatoes produced in Qingdao, Shandong province, China.

2.1 Test conditions and methods

2.1.1 Design of the geometric size and mass measuring

The design of soft end-effector was affected by the basic size and weight of tomatoes. Fifty tomatoes were randomly selected on December 25, 2020, and fifty tomatoes were randomly selected on July 21, 2021. The transverse diameter h_t, vertical diameter h_v, and height of maximum transverse diameter h_h of tomatoes were measured with a large range stainless steel vernier caliper (Nscing Es, China). h_t, h_v, and h_h were shown in Figure 1. The transverse diameter represented the maximum horizontal diameter of tomatoes. The vertical diameter represented the maximum vertical diameter of tomatoes. The stalks of tomatoes were placed vertically. The outer measuring jaw of the vernier caliper, whose length is 100mm, can accurately measure the size of tomatoes. The mass m of tomatoes was measured with electronic balance JA5001 (Puchun, China).

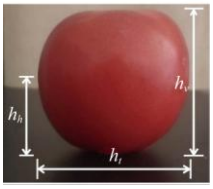

Figure 1 The geometric parameters of a tomato

2.1.2 Design of the static friction characteristic test

Ten tomatoes were randomly selected on December 25, 2020. The static friction characteristics of the tomatoes were tested on a silicone pad made of Dragon Skin 30. The thickness of the silicone pad was 3mm, same as that of the bottom layer of the designed end-effector. A tensile testing machine HY-0580 (Hengyi, China) and a fixed pulley were used. The test method was as follows: One tomato was weighed and placed on a silicone pad. The tomato, the fixed pulley, and the chuck of tensile tester were connected with a wire. The fixed pulley could convert the tensile force generated by the tensile testing machine from vertical to horizontal. The chuck of the tensile testing machine moved upward slowly. The moving speed of the chuck was set to 30 mm/min, which was within the quasi-static range. When the tomato was moved, the peak value of the pulling force was recorded. The test platform of the static friction characteristic is shown in Figure 2.

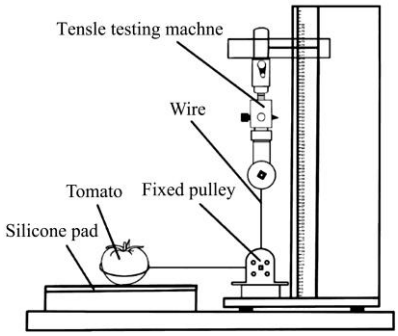

Figure 2 Test platform for the static friction characteristics

2.1.3 Design of the compression characteristic test

In order to study the stress tolerance, the stress test was performed on different parts of tomatoes. Twenty-five tomatoes were randomly selected on December 25, 2020. A TMS-TOUCH texture analyzer (FTC, USA) and a flat probe with a diameter of 50 mm working as the test probe were used. The probe was covered with a silicone pad made of Dragon Skin 30. The thickness of the silicone pad was 3 mm, the same as that of the bottom layer of the designed end-effector. The test platform is shown in Figure 3a.

The pressure-displacement test was carried out with the texture analyzer. The displacement was set to 20 mm, and the probe loading speed was 30 mm/min, which was within the quasi-static range. As shown in Figure 3b, five test points were selected for testing. Two adjacent test points were separated by 45°. The uppermost test point was defined as test point 1. The remaining test points were calibrated counterclockwise as test points 2, 3, 4 and 5. Test point 3 was the position of the maximum transverse diameter of the tomato.

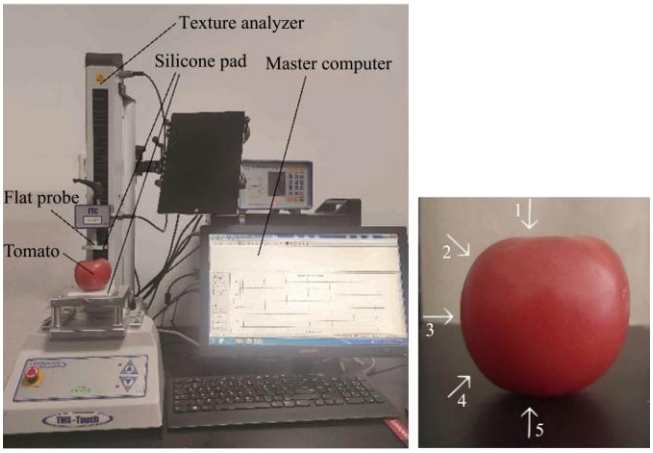

a. Test platform b. Test points

Figure 3 Test platform and test points for the compression characteristics

The test method is as follows: The test point of a tomato was determined by the protractor (Koslo, Germany). The tomato was fixed on the silicone pad with a thickness of 3mm, and the test point was vertically upward. The texture analyzer was driven to complete the test. Before the test, the tomato was fixed by two vertical baffles to prevent it from toppling. When the tomato was fixed and stabilized by the texture analyzer, the baffles would be

removed. Each position was tested 5 times.

2.1.4 Design of the damage characteristic test

Non-destructive clamping is an important research focus in designing an end-effector. There are two forms of mechanical damage to tomatoes[30]: When the tomato peel is not broken but the cell structure is destroyed, the enzymatic reaction will be triggered, making the color of the pressed parts become darker. When the tomato cells respirate fast, water inside the tomato will be lost, resulting in shrinking. In another case, the tomato peel is damaged, and the internal tissue is exposed. And then mildew appears on the surface of the tomato.

The damage of the finger made of Dragon Skin 30 to the tomato was verified by the damage characteristic test. Fifty-one tomatoes were randomly selected on July 21, 2021. The TMS-TOUCH texture analyzer (FTC, USA) was adopted for the test. A flat probe with a diameter of 50mm, covered with a silicone pad made of Dragon Skin 30 with a thickness of 3 mm, was used as the test probe. According to 2.2.3 Compression characteristics, test point 3 was selected as the test point. The applied variable was compression ratio, which was 0, 1%, 2%... 15%, and 16%. The compression ratio was the ratio of the compression distance to the transverse diameter of a tomato. Each case was tested three times. The probe's loading speed was 30 mm/min. The maximum pressures were recorded and the tomatoes were stored at room temperature. The average room temperature was 28℃. The number of days when tomatoes wrinkle or mildew was recorded.

2.2 Analysis of results of the physical property test

2.2.1 Geometric sizes and masses

The test results classified by the transverse diameter are shown in Table 1. The original data of geometrical sizes and masses of tomatoes are shown in Table 2. The results showed that the transverse diameter h_t was 63.8-89.7 mm, the vertical diameter h_v was 51.8-77.6 mm, the height of maximum transverse diameter h_h was 28.5-58.1 mm, and the mass m was 131.7-364.8 g. The opening diameter of the designed end-effector was greater than 90 mm.

Table 1 The masses for tested tomatoes in different size groups

Date	Size/mm	Percentage	Average mass/g	Maximum mass/g	Minimum mass/g
2020.12.25	60-65	2%	134.20	134.2	134.2
	65-70	12%	162.65	175.0	144.2
	70-75	40%	189.51	212.6	164.5
	75-80	28%	227.54	280.3	199.8
	80-85	16%	268.24	295.6	214.8
	85-90	2%	364.80	364.8	364.8
2021.7.21	60-65	4%	137.25	142.8	131.7
	65-70	16%	154.81	173.0	143.5
	70-75	46%	186.02	243.7	155.9
	75-80	24%	214.39	249.2	187.3
	80-85	8%	253.83	283.2	224.4
	85-90	2%	338.80	338.8	338.8

Table 2 Statistics for geometrical sizes and masses of tested tomatoes

Date	Tomato number	h_t/mm	h_v/mm	h_h/mm	m/g
2020.12.25	1	78.0	57.8	28.8	202.8
	2	72.0	63.4	39.7	183.5
	3	71.2	54.3	31.8	164.5
	4	89.7	75.0	54.3	364.8
	5	81.3	68.4	47.2	246.0
	6	74.5	60.0	45.2	181.1
	7	83.3	77.6	58.1	289.5
	8	69.3	67.6	57.2	175.0
	9	80.3	70.3	48.0	280.4
	10	73.6	63.4	39.2	204.7
	11	74.2	66.4	44.4	201.1
	12	73.2	61.9	45.0	181.8
	13	78.9	72.5	40.0	244.1
	14	78.6	64.5	43.8	229.2
	15	66.0	60.1	44.2	165.7
	16	74.6	70.5	43.3	203.7
	17	72.6	61.9	45.0	194.1
	18	66.9	55.2	34.9	144.2
	19	72.5	67.7	40.2	197.5
	20	80.1	71.8	46.7	253.2
	21	68.9	61.6	36.9	173.0
	22	81.5	74.3	50.4	274.1
	23	73.0	64.2	37.8	204.4
	24	79.6	61.6	34.2	215.2
	25	70.4	61.1	37.0	168.4
	26	68.0	59.1	40.1	156.7
	27	64.1	53.7	39.1	134.2
	28	79.2	68.3	37.9	245.7
	29	72.6	60.7	36.4	178.5
	30	76.1	66.0	45.3	199.8
	31	82.0	71.1	42.2	292.3
	32	74.1	65.5	45.5	194.8
	33	84.3	69.4	44.2	214.8
	34	77.2	64.7	38.4	224.4
	35	70.2	61.4	34.6	172.7
	36	78.4	72.1	47.7	251.2
	37	71.6	68.6	43.1	190.0
	38	72.5	61.2	48.7	189.1
	39	79.4	66.0	47.7	248.4
	40	84.0	70.3	45.7	295.6
	41	75.5	66.6	41.4	202.3
	42	73.0	65.0	41.6	183.0
	43	73.6	68.3	43.8	212.6
	44	78.6	62.1	39.6	204.6
	45	74.1	68.2	52.9	208.3
	46	79.6	71.4	46.1	280.3
	47	65.1	61.4	40.8	161.3
	48	75.7	71.0	39.3	212.8
	49	74.0	60.6	40.8	176.4
	50	76.6	68.4	42.2	224.8
2021.7.21	51	72.3	56.4	32.5	212.3
	52	72.5	60.2	35.5	243.7
	53	72.5	55.3	29.5	194.9
	54	75.9	64.4	41.3	236.5
	55	76.2	55.3	37.5	210.2
	56	74.3	56.0	34.5	182.4
	57	71.5	60.2	35.0	159.2
	58	80.9	63.5	47.3	261.2
	59	71.2	55.3	38.5	187.4
	60	66.2	56.2	35.2	151.3
	61	63.8	58.0	38.2	131.7
	62	81.6	61.5	37.2	246.5
	63	73.1	57.2	42.2	203.7
	64	77.1	58.2	39.8	218.1
	65	77.2	56.1	40.9	187.3
	66	72.1	56.1	35.0	169.2
	67	64.8	54.9	33.5	142.8
	68	65.0	51.8	28.5	143.5
	69	75.2	61.2	39.9	204.7
	70	72.0	67.2	46.8	193.7
	71	74.9	59.5	39.2	203.3
	72	77.9	65.9	45.2	219.7
	73	81.2	59.2	41.5	224.4
	74	65.9	56.8	40.2	155.7

Date	Tomato number	h_t/mm	h_v/mm	h_h/mm	m/g
2021.7.21	75	76.3	64.4	42.3	249.2
	76	68.2	61.5	40.1	173
	77	75.9	60.9	45.2	233.7
	78	79.0	60.8	36.9	188.2
	79	72.5	59.9	43.2	179.7
	80	72.5	54.3	40.2	171.3
	81	69.0	55.1	33.1	158.1
	82	87.4	73.5	45.5	338.8
	83	70.0	56.5	29.8	168.6
	84	84.5	68.0	40.9	283.2
	85	70.3	61.5	39.1	170.7
	86	76.0	60.9	35.2	203.8
	87	67.9	56.2	37.5	150.7
	88	72.3	61.8	41.8	176.9
	89	70.0	59.1	36.1	178.4
	90	67.5	58.5	32.1	160.6
	91	76.1	57.5	44.4	191.4
	92	70.9	55.0	29.0	155.9
	93	73.5	55.2	33.9	214.2
	94	66.0	54.0	30.5	145.6
	95	78.9	61.9	39.8	229.9
	96	70.9	52.8	36.1	158.4
	97	70.2	52.5	36.5	163.3
	98	72.5	64.3	34.5	221.1
	99	73.2	58.1	36.0	182.2
	100	73.9	60.0	37.3	188

2.2.2 Static friction characteristics

Based on the test results, the static friction characteristics of tomatoes on the Dragon Skin 30 material were solved by Equation (1):

$$\mu = \frac{\sum_{i=1}^{10} f_i}{\sum_{i=1}^{10} m_i g} \quad (1)$$

where, f_i, m_i, and g represent the maximum pulling force on a tomato, the mass of a tomato, and acceleration of gravity. The average pulling force was 2.881 N, and the average tomato mass was 208.39 g, and g is 9.8 N/kg. The calculated static friction coefficient was 1.41 N/N.

Table 3 The static friction characteristics of tomatoes

Tomato number	Pulling force/N	Mass/g	Static friction coefficient/N N^{-1}
1	2.921	212.8	1.40
2	2.865	175.8	1.66
3	2.904	227.8	1.30
4	2.572	167.4	1.57
5	3.232	276.8	1.19
6	2.825	204.6	1.41
7	2.986	221.4	1.38
8	2.62	149.6	1.79
9	3.123	276.1	1.15
10	2.762	171.6	1.64
Average	2.881	208.39	1.41

2.2.3 Compression characteristics

The pressure-displacement curve of a tomato is shown in Figure 4. The pressure-displacement curve of tomatoes initially showed an S-shaped curve. After the pressure exceeded the maximum value, the curve oscillated and the pressure decreased rapidly. The compression process was divided into three stages: elastic compression stage, damage stage, and rupture stage. The elastic compression stage was in the range of d<12.5 mm. At this stage, the curve was concave and the derivative of the curve function was greater than zero. The damage stage was 12.5<d< 17.5 mm. At this stage, the curve was convex and the deformation of the tomato was significant. When the rupture stage was reached, tomatoes were macroscopically fractured. The maximum value of pressure was the rupture force F_b of tomatoes.

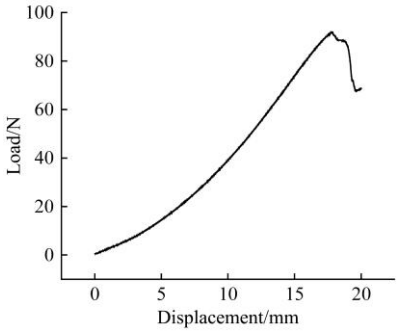

Figure 4 Pressure-displacement curve of a tomato

The statistics for the rupture force of tomatoes are shown in Table 4. The effects of mass, test point, and transverse diameter on rupture force values were evaluated by analysis of variance and the results were examined at 95% confidence level. The results of variance analysis are shown in Table 5. The P-values of the three factors were greater than 0.05. There was no correlation between the test point, the mass, the size and the rupture force of tomatoes. The average rupture force of the tomato at test point 3 was the smallest, and the average rupture force of the tomato at test point 5 was the largest. Therefore, test point 3 was selected as the stress point for subsequent tests and simulations to ensure that the tomato would not be damaged by the end-effector in practice.

Table 4 The rupture force of tomatoes

Test point	Tomato number	Transverse diameter/mm	Mass/g	Rupture force/N	Average rupture force/N
1	1	73.6	204.66	120.07	111.79
	2	73.2	181.78	103.47	
	3	74.2	201.12	125.97	
	4	79.6	215.21	116.14	
	5	73.0	182.98	93.32	
2	1	83.3	289.48	121.15	112.79
	2	65.1	161.25	92.84	
	3	69.3	175.02	113.12	
	4	72.6	178.46	124.42	
	5	73.0	204.39	112.41	
3	1	72.0	183.51	88.02	96.27
	2	68.0	156.65	83.52	
	3	89.7	364.80	92.01	
	4	74.0	176.42	105.83	
	5	80.1	253.21	111.96	
4	1	78.9	244.08	142.48	111.58
	2	70.2	172.65	110.43	
	3	66.0	165.73	108.86	
	4	79.4	248.42	101.32	
	5	74.6	203.66	94.81	
5	1	71.6	190.04	147.90	130.62
	2	74.5	181.13	112.54	
	3	66.9	144.17	119.17	
	4	81.3	245.96	129.35	
	5	72.5	197.48	144.13	

Table 5 Analysis of variance of the compression characteristic test

Source	Sum of Squares	*df*	Mean square	*F*-value	*p*-value
Model	321096.951[a]	12	26758.079	113.269	0.000
Test Point	2421.105	4	605.276	2.562	0.088
h_t	364.717	3	121.572	0.515	0.679
m	191.106	3	63.702	0.270	0.846
Error	3071.049	13	236.235		
Total	324168.000	25			

Note: a. R^2 = 0.991 (Adjusted R^2 = 0.982); h_t: the transverse diameter of tomatoes; *m*: the mass of tomatoes. Dependent variable: rupture force

2.2.4 Damage characteristics

In the damage characteristic test, stressed tomatoes were used as experimental samples, and unstressed tomatoes as reference samples. The test results are shown in Table 6. The effects of compression force, transverse diameter, and mass on number of days were evaluated by analysis of variance and the results were examined at 95% confidence level. The results of variance analysis are shown in Table 7. The P-value of compression force was less than 0.05. There was a significant relationship between the compression force and the storage days of tomatoes. The *p*-values of transverse diameter and mass were greater than 0.05. There was no correlation between the transverse diameter, the mass and the storage days of tomatoes. The number of days when the reference samples wrinkled or mildewed was more than 10 d. Due to individual differences in tomatoes, 9 d was used as the judgment value that tomatoes were clamped without damage. The results showed that the greater the compression force, the shorter the storage days of tomatoes. When the compression force was less than 11.13 N, the storage time of tomatoes was more than 9 d. In order to clamp tomatoes without damage, the force on the tomatoes should be less than 11.13 N.

Table 6 Results of the damage characteristic test

Compression percentage/%	Tomato number	Transverse diameter/mm	Mass/g	Compression force/N	Number of days
0	1	76.1	191.4	0	11
	2	70.9	155.9	0	13
	3	73.5	214.2	0	10
1	1	75.2	204.7	3.59	11
	2	72.0	193.7	3.96	13
	3	72.5	179.7	2.99	12
2	1	73.2	182.2	4.82	10
	2	72.3	176.9	5.64	11
	3	67.9	150.7	4.67	12
3	1	72.5	171.3	6.95	10
	2	81.2	224.4	6.20	12
	3	65.9	155.7	5.57	11
4	1	70.9	158.4	8.33	10
	2	70.2	163.3	9.12	13
	3	73.9	188.0	11.13	13
5	1	64.8	142.8	9.79	9
	2	65.0	143.5	10.27	10
	3	76.3	249.2	7.36	14
6	1	76.0	185.2	12.74	8
	2	71.5	159.2	10.16	11
	3	80.9	261.2	19.46	10
7	1	68.2	173.0	15.62	9
	2	69.0	158.1	17.75	8
	3	75.9	233.7	24.13	9
8	1	72.3	212.3	19.39	8
	2	72.5	243.7	24.69	13
	3	73.1	203.7	19.28	12
9	1	79.0	188.2	13.30	8
	2	74.9	203.3	23.05	12
	3	77.9	219.7	17.07	5
10	1	77.1	218.1	24.17	11
	2	71.2	187.4	16.66	7
	3	66.2	151.3	19.73	15
11	1	70.0	178.4	35.68	7
	2	67.5	160.6	27.27	10
	3	70	168.6	24.36	13
12	1	72.5	194.9	27.27	7
	2	75.9	236.5	49.72	7
	3	87.4	338.8	47.93	11
13	1	84.5	283.2	53.87	6
	2	66.0	145.6	38.22	8
	3	78.9	229.9	27.98	9
14	1	77.2	187.3	29.81	7
	2	72.1	169.2	41.73	12
	3	63.8	131.7	34.82	6
15	1	70.3	170.7	48.34	10
	2	76.0	203.8	36.16	4
	3	72.5	221.1	34.07	8
16	1	81.6	246.5	49.99	10
	2	76.2	210.2	51.18	8
	3	74.3	182.4	50.99	6

Table 7 Analysis of variance of the damage characteristic test

Source	Sum of squares	*df*	Mean square	*F*-alue	*p*-value
Model	5115.806[a]	25	204.632	55.309	0.000
Compression force	105.435	11	9.585	2.591	0.023
h_t	17.119	4	4.280	1.157	0.353
m	21.644	8	2.705	0.731	0.663
Error	96.194	26	3.700		
Total	5212.000	51			

Note: a. R^2 = 0.982 (Adjusted R^2 = 0.964); h_t: the transverse diameter of tomatoes; *m*: the mass of tomatoes; Dependent variable: number of days.

3 Design, simulation and optimization of the end-effector

3.1 Design of the flexible finger structure

Figure 5 shows the multi-chamber flexible finger designed in this paper. A single flexible finger was composed of the chamber structure and the bottom layer. Before clamping, the flexible fingers were driven by negative pressure. In this case, the pressure inside the chambers was lower than the outside pressure. So the flexible fingers bent in reverse. This method increases the opening diameter of the end-effector and the tolerance of the visual positioning system. The chambers of the fingers were inflated when the end-effector was moved to the proper position. After the inflation, the chambers expanded as the pressure inside the chambers was greater than the pressure outside the chambers. And then the flexible fingers bent toward the bottom layer for clamping.

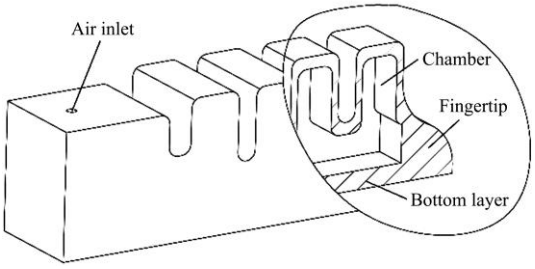

Figure 5 The flexible finger

3.2 Finite element analysis of the flexible finger

3.2.1 Design of the bending simulation

The flexible fingers worked by being bent towards the bottom layer. The clamping ability of the end-effector was affected by the bending performance of the flexible fingers. In this paper, static analysis module in Ansys Workbench was used to simulate and analyze the model. The tested models were 4-chamber, 5-chamber, and 6-chamber flexible fingers. The material of the flexible fingers was Dragon Skin 30. According to the research of Michigan State University[31], the Ogden model with parameter values D=1, α_1=2.7172, μ_1=0.1581 MPa was the best constitutive model. D, α, μ respectively represent the incompressible parameter, the strain hardening exponent, and the shear modulus of the material. Hex Dominant was used for meshing. Hex Dominant can perform finite element analysis on the force and deformation of silicone. Press was applied to the inner surface of the flexible finger. The pressure was set to 15, 20, 25, 30, 35, 40, 45 kPa. Through the Directional Deformation in the post-processing, the horizontal and vertical displacements of the bottom surface of the flexible finger were obtained. Figure 6 shows the deformation of the flexible fingers with 4, 5, and 6 chambers at 30 kPa.

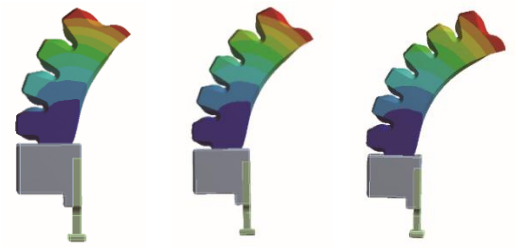

a. 4-chamber b. 5-chamber c. 6-chamber

Figure 6 Simulation results of the flexible fingers at 30 kPa

3.2.2 Design of the clamping simulation

The clamping force of the end-effector was affected by the number of chambers of the flexible fingers and the inflation pressure. The number of finger chambers (4, 5, 6) and the inflation pressure (15, 20, 25, 30, 35, 40, 45 kPa) were used as variables to simulate tomatoes with different diameters. The effects of the number of finger chambers and the diameter of tomatoes on the clamping force were studied. The measured transverse diameter was 63.8-89.7 mm, so 65, 75, and 85 mm were used as the tomato sizes for modeling. According to 2.2.1 Geometric sizes and masses, the initial opening diameter of the end- effector was 90 mm. As being at a negative pressure state before clamping, the end-effector with an opening diameter of 90 mm was sufficient to hold the largest tomato.

The relevant parameters of clamping simulation were the same as deformation simulation. Contact was added between the flexible finger and the tomato. In post-processing, Force Reaction was used to check the force of the tomato. The total force, horizontal force, and vertical force of tomatoes in each group were recorded and analyzed. Figure 7 shows that a flexible finger with 4 chambers held a tomato with a transverse diameter of 75 mm at 30 kPa.

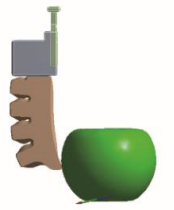

Figure 7 The four-chamber finger held tomato at 30 kPa

3.3 Analysis of simulation results

3.3.1 Results of the bending simulation

Figure 8 shows the bottom surface displacement of flexible fingers with different numbers of chambers at 15-45 kPa, including horizontal displacement D_x and vertical displacement D_z. The horizontal and vertical displacements of the fingers with different numbers of chambers were proportional to the inflation pressure.

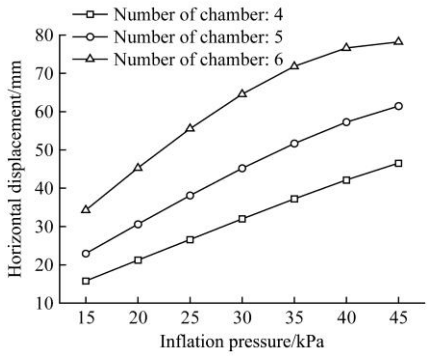

a. Horizontal direction

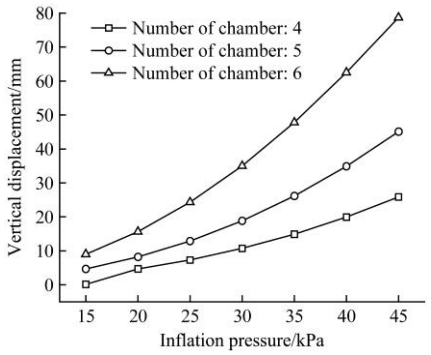

b. Vertical direction

Figure 8 Results of the deformation simulation

The derivative of the horizontal displacement function was less than zero. When the inflation pressure p > 35 kPa, the horizontal displacement curve of the 6-chamber finger became flat. It showed that the 6-chamber finger was close to the limit of horizontal elongation. The 4-chamber and 5-chamber fingers did not reach the limit of horizontal elongation at the inflation pressure of 15-45 kPa. The ultimate inflation pressure was an important parameter of a flexible finger. The horizontal displacement of the finger corresponding to the ultimate inflation pressure determines the minimum size of the object clamped by the end-effector. When the inflation pressure was less than the ultimate inflation pressure, the minimum size of the object clamped by the end-effector decreased as the inflation pressure increased. When the inflation pressure was greater than the ultimate inflation pressure, the minimum size of the object clamped by the end-effector remained the same as the inflation pressure increased.

The derivative of the vertical displacement function was greater than zero. It showed that when the inflation pressure was small, the fingers were mainly bent horizontally. When the inflation pressure gradually increased, the deformation of the finger gradually shifted to the vertical direction.

The deformability of the fingers was proportional to the number of chambers. When the inflation pressure was 15 kPa, the horizontal deformation displacement of the 4-chamber finger was 15.794 mm. The transverse diameter of the smallest tomato was 64.1 mm. The end-effector with a radius of 90 mm was capable of generating clamping forces on tomatoes of all sizes at an inflation pressure greater than 15 kPa.

3.3.2 Results of the clamping simulation

The effects of number of finger chambers, transverse diameter, and inflation pressure on horizontal force values, vertical force values, and total force values were evaluated by analysis of variance and the results were examined at 95% confidence level. The results of variance analysis are shown in Table 8. The *p*-values of all factors were less than 0.05. There were statistically significant correlations between the number of finger chambers, the transverse diameter, the inflation pressure and the three clamping forces.

Table 8 Analysis of variance of the clamping simulation

Source	Dependent variable	Sum of squares	*df*	Mean square	*F*-value	*p*-value
Model	Horizontal force	41.120[a]	11	3.738	774.978	0.000
	Vertical force	2.255[b]	11	0.205	109.107	0.000
	Total force	43.507[c]	11	3.955	927.234	0.000
Number of finger chambers	Horizontal force	0.109	2	0.055	11.312	0.000
	Vertical force	0.031	2	0.016	8.322	0.001
	Total force	0.128	2	0.064	15.019	0.000
Transverse diameter	Horizontal force	0.215	2	0.108	22.318	0.000
	Vertical force	0.019	2	0.010	5.098	0.010
	Total Force	0.225	2	0.112	26.341	0.000
Inflation pressure	Horizontal force	8.266	6	1.378	285.595	0.000
	Vertical force	0.711	6	0.119	63.125	0.000
	Total force	8.960	6	1.493	350.103	0.000
Error	Horizontal force	0.251	52	0.005		
	Vertical force	0.098	52	0.002		
	Total force	0.222	52	0.004		
Total	Horizontal force	41.371	63			
	Vertical force	2.352	63			
	Total force	43.729	63			

Note: a. R^2 = 0.994 (Adjusted R^2 = 0.993); b. R^2 = 0.958 (Adjusted R^2 = 0.950); c. R^2 = 0.995 (Adjusted R^2 = 0.994)

Figure 9 shows the variation of the horizontal force, the vertical force and the total force with the inflation pressure when the number of finger chambers was 4 and the size of tomatoes was 75 mm. The total clamping force, the horizontal force, and the vertical force were directly proportional to the inflation pressure. The total clamping force and the horizontal force increased linearly. The vertical force increased exponentially. This was determined by the bending characteristics of the flexible fingers. As the inflation pressure increased, the clamping position of the flexible finger holding tomatoes remained unchanged, but the angle between the total clamping force and the horizontal direction gradually increased.

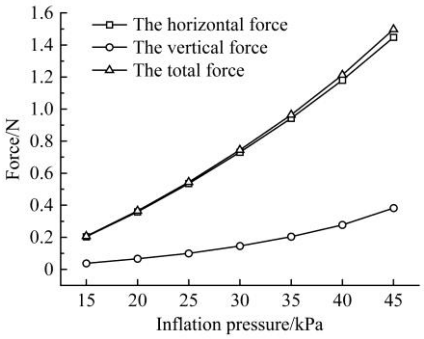

Figure 9 Horizontal force, vertical force and total force under the same conditions

The clamping force-inflation pressure curves of the flexible finger are shown in Figure 10.

When the inflation pressure was less than 35 kPa, the number of chambers was directly proportional to the total clamping force. When the inflation pressure was greater than 35 kPa, the number of chambers was inversely proportional to the total clamping force. The number of chambers was inversely proportional to the slope of the horizontal force-pressure curve. The number of chambers was directly proportional to the angle between the total clamping force and the horizontal direction. The reason was that fingers with more chambers had higher flexibility. When the distance from the fingertip to the contact point between the finger and the fruit was constant, the more the number of chambers in the finger, the more energy generated by the pressure difference was transformed into the bottom layer deformation.

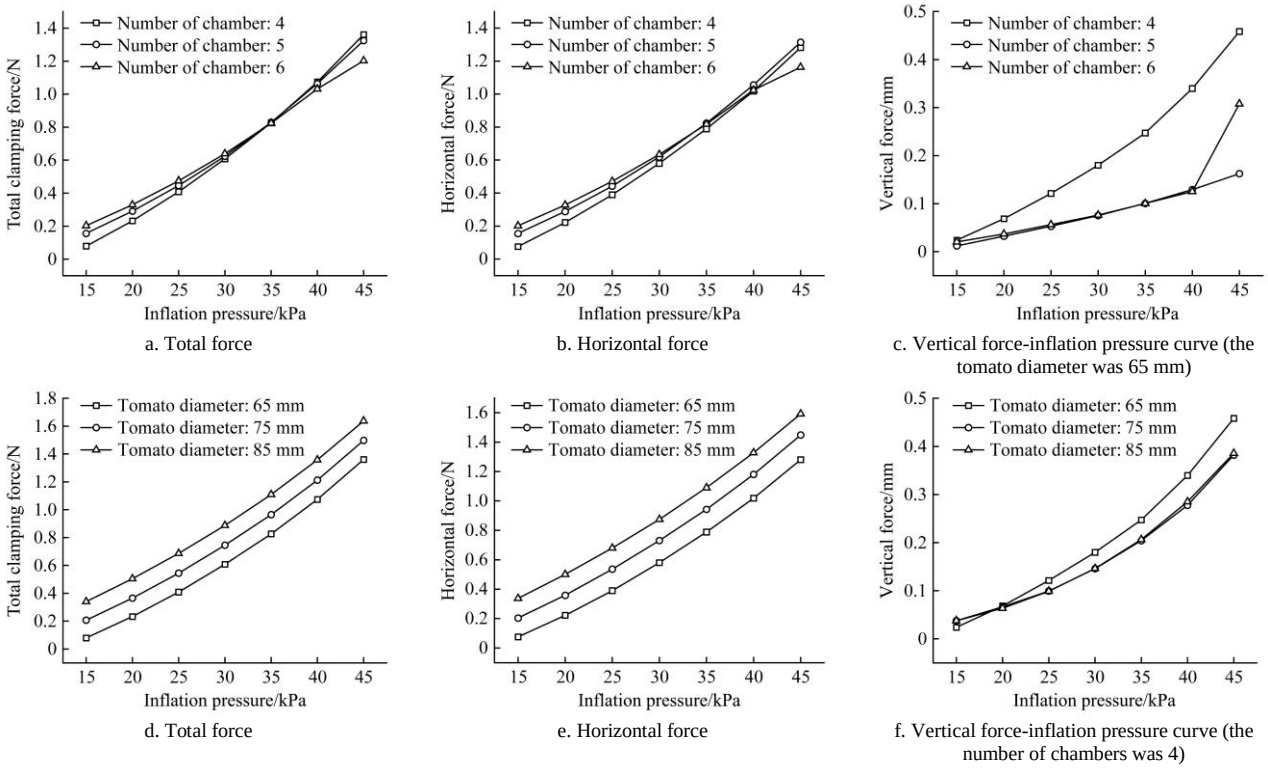

a. Total force b. Horizontal force c. Vertical force-inflation pressure curve (the tomato diameter was 65 mm)

d. Total force e. Horizontal force f. Vertical force-inflation pressure curve (the number of chambers was 4)

Figure 10 Results of the clamping simulation

When the number of chambers remained constant, the size of tomatoes was directly proportional to the total and horizontal clamping forces. When the inflating pressure was less than 20 kPa, the vertical force was less affected by the size of tomatoes. When the inflation pressure was greater than 20 kPa, the vertical force was significantly affected by the size of tomatoes. When the inflation pressure was high, the vertical force exerted by the fingers on a tomato with a diameter of 65 mm was significantly greater than that on a tomato with a larger size. The reason was that when the size of the tomato was smaller, the deformation of the finger was greater. The vertical force was proportional to the deformation of the finger.

3.4 Flexible finger optimization based on genetic algorithm

Genetic algorithm is a method to search for the optimal solution by simulating the natural evolution process. Based on the working requirements, the optimal solutions for the number of chambers, the number of fingers, and inflation pressure were obtained by genetic algorithm. The energy consumption and the production cost were used as optimization parameters to reduce the cost of the end-effector.

Genetic algorithm in Optimization Tool of Matlab was used for optimization. The boundary conditions of the relevant variables were as follows:

$$\begin{cases} n = 4,5,6 \\ k = 2,3,4 \\ 15\ \text{kPa} \le p \le 45\ \text{kPa} \\ \mu k F_x + k F_z \ge mg \end{cases} \quad (2)$$

where, n, k, p, F_x, F_z, and m represent number of chambers of a flexible finger, number of flexible fingers of end-effector, inflation pressure, horizontal force generated by flexible finger, vertical force generated by flexible finger, and mass of tomatoes. From the geometric size and mass test, various-sized tomatoes are different in their masses. The geometric size of tomatoes was divided into sections. One hundred samples were tested for sizes and masses, and special samples cannot be ruled out. Since tomatoes with a size of 60-65 mm and 85-90 mm accounted for a small proportion, tomatoes outside the range of 60-90 mm were not considered. When the size was constant, the mass was directly proportional to the difficulty of clamping. Therefore, the maximum size of tomatoes in each group was increased by 10% and rounded as the optimization parameter. In the simulation, when d was 65 mm, m was 200 g (when d = 60-70 mm, m_{max} = 175 g); when d was 75 mm, m was 300 g (when d = 70-80 mm, m_{max} = 280.3 g); when d was 85 mm, m was 400 g (when d = 80-90 mm, m_{max} = 364.8 g). From the tomato static friction characteristic test, μ = 1.41 N/N. g is 9.8 N/kg.

In order to set the fitness function, the energy consumption and the production cost were normalized. The square sum of the energy consumption and the production cost were taken as the fitness function.

$$\begin{cases} p = \dfrac{p - p_{min}}{p_{max} - p_{min}} \\ V = \dfrac{kv - 2 \times V_{min}}{4 \times V_{max} - 2 \times V_{min}} \end{cases} \quad (3)$$

$$fun = p^{-2} + V^{-2} \quad (4)$$

where, p_{min} and p_{max} represent the minimum and the maximum inflation pressure used in the clamping simulation; V_{min} and V_{max} represent the minimum and maximum volume of a flexible finger. According to the finger model in UG, when n=4, V= 33.4552836 cm^3; when n=5, V=38.0302836 cm^3; when n=6, V= 42.6005236 cm^3.

The results of clamping simulation were collated and fitted to get the horizontal force and vertical force functions of a single finger under different conditions. Equations (5) and (2) were combined to set the nonlinear constraint function of the genetic algorithm.

$$\begin{cases} n=4,\ d=65\ \text{mm},\ F_x = 0.0401p - 0.5795,\ F_z = 0.0094\text{e}^{0.0913p} \\ n=4,\ d=75\ \text{mm},\ F_x = 0.0413p - 0.468,\ F_z = 0.0141\text{e}^{0.0752p} \\ n=4,\ d=85\ \text{mm},\ F_x = 0.0416p - 0.3343,\ F_z = 0.0136\text{e}^{0.0764p} \\ n=5,\ d=65\ \text{mm},\ F_x = 0.0385p - 0.4836,\ F_z = 0.0055\text{e}^{0.0803p} \\ n=5,\ d=75\ \text{mm},\ F_x = 0.0346p - 0.3349,\ F_z = 0.0142\text{e}^{0.077p} \\ n=5,\ d=85\ \text{mm},\ F_x = 0.0349p - 0.2627,\ F_z = 0.0134\text{e}^{0.0755p} \\ n=6,\ d=65\ \text{mm},\ F_x = 0.033p - 0.3278,\ F_z = 0.0067\text{e}^{0.0799p} \\ n=6,\ d=75\ \text{mm},\ F_x = 0.0309p - 0.2713,\ F_z = 0.0053\text{e}^{0.0928p} \\ n=6,\ d=85\ \text{mm},\ F_x = 0.03p - 0.2138,\ F_z = 0.0116\text{e}^{0.0795p} \end{cases} \quad (5)$$

In the Options module, set the Population size to 100, the Elite count to 10, the Crossover fraction to 0.75, and the Generations to 50. The results are shown in Figure 11.

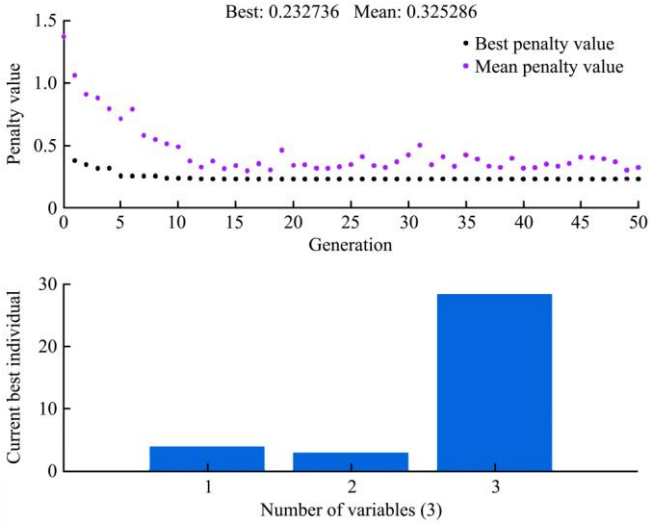

Figure 11 Optimization results of the genetic algorithm

After the genetic generation reached 10 generations, the penalty value approached the optimal value. The optimal number of chambers, number of fingers, and inflation pressure are 4, 3, and 28.293 kPa. The optimized structure was an end-effector composed of three four-chamber fingers, and the optimal inflation pressure was 28.293 kPa. According to 3.3.2 Results of the clamping simulation, when the inflation pressure was less than 28.293 kPa, the clamping force was significantly less than the damage force of 11.13 N. Tomatoes will not be damaged by the end-effector.

4 Experimental validation

4.1 Fabrication

The silicone material of the flexible end-effector was Dragon Skin 30. The flexible finger was fabricated by shape deposition manufacturing method. The mold in this paper was modeled by UG and made by 3D printing, including the chamber bottom mold, the chamber cover mold, and the bottom mold. The procedure of fabrication process is described as follows:

1) The A and B liquids of Dragon Skin 30 were mixed and stirred; 2) The mold surface was coated with petroleum jelly to

facilitate demolding; 3) The mixed liquid Dragon Skin 30 was poured into the chamber bottom mold; 4) The chamber bottom mold was placed at a low temperature for 30 min to remove air bubbles; 5) The chamber cover mold was put on the chamber bottom mold and fixed; 6) After one hour, the finished chamber part of the flexible finger was taken out; 7) The A and B liquids of Dragon Skin 30 were mixed and stirred again, and the Dragon Skin 30 was poured into the bottom mold; 8) The bottom mold was placed at a low temperature for 30 min, then the finished chamber part was placed on the surface of the bottom mold; 9) After one hour, the flexible finger was obtained. The mold and the finished flexible finger are shown in Figure 12.

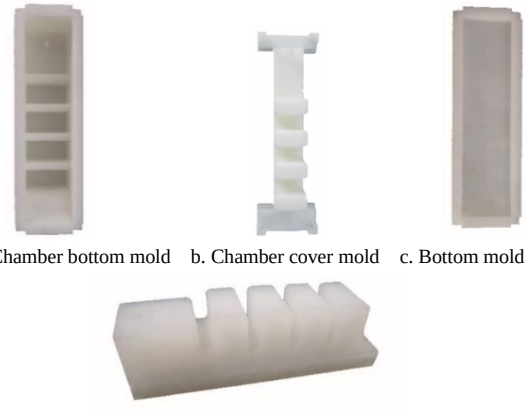

a. Chamber bottom mold b. Chamber cover mold c. Bottom mold

d. Flexible finger

Figure 12 The mold and the flexible finger

4.2 Tests of the flexible end-effector

4.2.1 Design of the bending test

The performance of the flexible finger was verified by finger bending test. During the test, the end of the flexible finger was fixed horizontally. The inflation pressure was 15-45 kPa. The air source was the active driver ACU-V1.3 (Rochu, China). The images of the flexible finger in the inflated state were recorded. The bending angles of the flexible finger at different inflation pressures were obtained by post-processing. The image was copied to CAXA. A straight line was used to connect the root of the finger to the tip of the finger in CAXA. Then the angle of the line to the horizontal direction was measured. Figure 13 shows the inflatable state of the flexible finger and the bending angle α. The test results were compared with the simulation results to verify the rationality of the simulation.

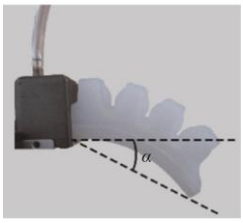

Figure 13 The inflated flexible finger

4.2.2 Design of the static clamping test

The static clamping performance was verified by the static clamping test. Thirty tomatoes were randomly selected on July 21, 2021. The test steps were shown in Figure 14. The end-effector and the industrial manipulator SV45 (APE, China) were assembled. The flexible end-effector was controlled to clamp tomatoes at different inflation pressures. The air source was the active driver ACU-V1.3 (Rochu, China). After the tomato was clamped by the inflated end-effector, the end-effector was moved vertically up 10cm by the manipulator. The movement speed was 1% of the maximum speed of the industrial manipulator, which was 6 cm/s. The tomato was successfully clamped when held for 5 seconds without falling. The inflation pressure was 15-45 kPa. The minimum inflation pressures for successfully clamping tomatoes of different sizes and masses were recorded. After the test, the tested tomatoes were placed at room temperature. The average room temperature was 28 ℃. The number of days when tomatoes wrinkle or mildew was recorded.

a. Preparation b. Pre-clamping c. Clamping d. Remaining e. Placement

Figure 14 Steps of the static clamping test

4.2.3 Design of the dynamic clamping test

The dynamic clamping performance was verified by the dynamic clamping test. Thirty tomatoes were randomly selected on July 21, 2021. The test was carried out by simulating the working environment of the sorting robot. The test steps were shown in Figure 15. The end-effector and the industrial manipulator SV45 (APE, China) were assembled. The end-effector was moved to the clamping position and clamped the tomato. The end-effector was moved vertically by the manipulator for 10 cm and horizontally for 30 cm. The tomato was placed on the table by the end-effector. When the tomato was clamped by the inflated end-effector and did not fall off during the test, the tomato was successfully clamped. The air source was the active driver ACU-V1.3 (Rochu, China). Since the inflation pressure can only be set as an integer, the inflation pressure was 29 kPa. The movement speed of the end-effector was 10% of the maximum speed of the industrial manipulator, which was 60cm/s. Thirty tomatoes were tested. After the test, the tested tomatoes were placed at room temperature. The average room temperature was 28 ℃. The number of days when tomatoes wrinkle or mildew was recorded.

4.3 Results of the flexible end-effector tests

4.3.1 Results of the bending test

The test results and the simulation results of bending performance were shown in Figure 16. The inflation pressure was set as the horizontal axis, and the bending angle α of the flexible finger as the vertical axis. The trend of the test results was similar to the simulation results. When the inflation pressure was less than 30 kPa, the test results were almost the same as the simulation results. When the inflation pressure was greater than 30 kPa, the test bending angle was obviously smaller than the simulation bending angle. The error was less than 3 °.

a. Preparation b. Pre-clamping c. Clamping d. Lifting

e. Moving f. Pre-placement g. Placement h. End

Figure 15 Steps of the dynamic clamping test

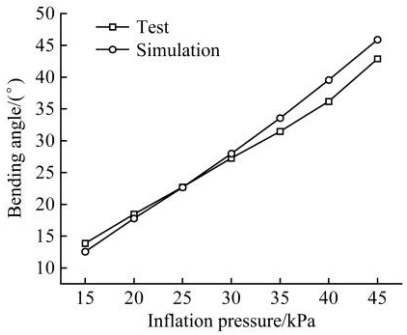

Figure 16 Test results and the simulation results of bending performance

4.3.2 Results of the static clamping test

The results of the static clamping test are shown in Table 9. The transverse diameter of the tested tomatoes was 65.9-82.1 mm, and the mass was 145.2-281.3 g. The results showed that the minimum inflation pressures of the test were less than 28.293 kPa. The effects of transverse diameter and mass on minimum inflation pressure values were evaluated by analysis of variance and the results were examined at 95% confidence level. The results of variance analysis are shown in Table 10. The *p*-values of both factors were less than 0.05. The transverse diameter and the size were correlated with the minimum inflation pressure. The end-effector optimized by genetic algorithm could hold tomatoes under static situation at the inflation pressure of 28.293 kPa. The storage days of the tested tomatoes were more than 9 d. The tomatoes were not damaged during clamping.

4.3.3 Results of the dynamic clamping test

The parameters of the tomatoes used in the dynamic clamping test are shown in Table 11. The transverse diameter of the tested tomatoes was 64.3-85.7 mm, the mass was 148.5-304.9 g. The tomato No.10 fell during the test because the placement position of the tomato deviated from the center of the clamping position. The test was successful after the tomato was repositioned. The success rate of the dynamic clamping test was 97%. The storage days of the tested tomatoes were more than 9 d. The tested tomatoes were not damaged. The optimized parameters were effective.

Table 9 Results of the static clamping test

Tomato number	Transverse diameter/mm	Mass/g	Minimum Inflation pressure/kPa	Number of days
1	72.7	221.5	25	12
2	71.2	197.3	24	11
3	73.3	218.5	24	10
4	70.2	198.9	25	13
5	82.1	281.3	26	10
6	76.5	232.5	25	12
7	74.9	221.7	24	13
8	67.2	162.8	26	10
9	74.3	224.1	23	10
10	66.2	159.0	25	12
11	78.2	242.3	25	11
12	81.4	238.4	23	10
13	66.0	152.4	26	9
14	77.6	245.8	24	14
15	72.3	187.2	24	10
16	73.0	198.8	23	13
17	76.5	217.6	26	10
18	71.2	203.2	24	12
19	65.9	163.5	27	11
20	78.5	198.9	23	9
21	72.2	172.7	23	13
22	76.1	195.4	24	11
23	70.2	176.5	24	10
24	69.1	162.2	25	12
25	70.8	192.3	26	15
26	71.2	167.2	24	10
27	67.3	145.6	23	12
28	73.2	162.3	24	11
29	72.5	216.8	26	10
30	76.4	195.0	25	11

Table 10 Analysis of variance of the static clamping test

Source	Sum of squares	df	Mean square	*F*-value	*p*-value
Model	18091.549[a]	23	786.589	2246.579	0.000
h_t	19.944	11	1.813	5.178	0.019
m	14.716	9	1.635	4.670	0.027
Error	2.451	7	0.350		
Total	18094.000	30			

Note: a. R^2 = 1.000 (Adjusted R^2 = 0.999); h_t: the transverse diameter of tomatoes; *m*: the mass of tomatoes. Dependent variable: minimum inflation pressure

Table 11 The tested tomatoes of the dynamic clamping test

Tomato number	Transverse diameter/mm	Mass/g	Number of days
1	72.3	205.8	10
2	74.6	187.2	12
3	77.1	226.5	13
4	71.0	190.0	10
5	68.5	153.6	10
6	72.1	201.2	11
7	82.6	251.7	12
8	72.8	176.5	11
9	78.1	243.2	12
10	70.4	172.3	9
11	75.6	216.8	10
12	80.2	235.7	11
13	66.4	165.9	12
14	74.1	201.3	12
15	73.8	196.5	11
16	85.7	304.9	9
17	73.5	182.3	13
18	75.0	208.4	14
19	71.1	176.5	10
20	68.2	161.0	13
21	72.2	182.4	11
22	64.3	148.5	16
23	78.8	256.3	10
24	75.7	215.0	14
25	74.6	201.6	11
26	70.9	172.1	9
27	69.5	173.6	13
28	75.9	213.5	10
29	81.2	261.7	15
30	73.9	205.9	11

5 Conclusions

The physical characteristics of tomatoes were tested. The flexible finger of the end-effector was modeled by UG and simulated by Ansys. The end-effector was designed by genetic algorithm according to the physical characteristics of tomatoes and the simulation results of the finger. The end-effector could hold tomatoes of different sizes and different masses at a low cost.

Through the physical characteristics test, the transverse diameter of tomatoes was 63.8-89.7 mm and the mass was 131.7-364.8 g. The static friction coefficient of the tomatoes on the silicone pad made of Dragon Skin 30 was 1.41 N/N. There was no correlation between the test point, the mass, the size and the rupture force of tomatoes. The non-destructive clamping force of tomatoes was 11.13 N.

The clamping range of the end-effector was determined after the simulation of flexible fingers. There were statistically significant correlations between the number of finger chambers, the transverse diameter of tomatoes, the inflation pressure and the clamping force. With the increase of inflation pressure, the total clamping force and the horizontal force increased linearly, and the vertical force increased exponentially. Since fingers with more chambers had higher flexibility, the number of chambers was inversely proportional to the slope of the horizontal force-pressure curve, and the number of chambers was directly proportional to the angle between the total clamping force and the horizontal direction. The size of tomatoes was directly proportional to the total and horizontal clamping forces.

The designed end-effector composed of three four-chamber fingers could hold tomatoes under static situation at the inflation pressure of less than 28.293 kPa. The end-effector clamped tomatoes under dynamic situation at the inflation pressure of 29 kPa, and the dynamic clamping success rate was 97%. The tested tomatoes were not damaged.

Acknowledgements

This work was supported by Jiangsu Agricultural Science and Technology Innovation Fund (CX (21) 1007).

[References]

[1] Wang T, Ye H, Zheng J, Li M. Research progress of main flavor compounds in tomato fruits. Acta Agriculturae Zhejiangensis, 2020; 32(8): 1513–1522. (in Chinese)

[2] Ullah I, Mao H, Zhang C, Javed Q, Azeem A. Optimization of irrigation and nutrient concentration based on economic returns, substrate salt accumulation and water use efficiency for tomato in greenhouse. Archives of Agronomy and Soil Science, 2017; 63(2): 1748–1762.

[3] Owusu J, Ma H, Wang Z, Afoakwah N A, Amissah A. Volatile profiles of tomato wine before and after ageing. Maejo International Journal of Science and Technology, 2014; 8(2): 129–142.

[4] Du R, Kou Y, Zhu L. Bibliometric analysis of literature in Chinese Core Journals from 1999 to 2019 with tomato as research topics and hotspots. China Vegetables, 2020; 11: 85–91. (in Chinese)

[5] Liu C, Han X, Cai L, Lu X, Ying T, Jiang Z. Postharvest UV-B irradiation maintains sensory qualities and enhances antioxidant capacity in tomato fruit during storage. Postharvest Biology and Technology, 2011; 59(3): 232–237.

[6] Wang Q, Wang J, Su X, Li W, Cao J, Jin K, et al. Evaluation and selection experiment of tomato varieties in dryland. Journal of Shanxi Agricultural Sciences, 2020; 48(8): 1247–1249, 1297. (in Chinese)

[7] Shang L, Song J, Wang J, Zang Y, Ye Z. Research progress on quality formation and molecular mechanism of tomato fruit. China Vegetables, 2019; 4: 21–28. (in Chinese)

[8] Preter A D, Anthonis J, Baerdemaeker J D. Development of a robot for harvesting strawberries. IFAC PapersOnLine, 2018; 51(17): 14–19.

[9] Chen Z, Jiang S, Sun Y. Development status of agroforestry harvesting robots. Agricultural Engineering, 2019; 9(02): 10–18. (in Chinese)

[10] Wang G, Yu Y, Feng Q. Design of end-effector for tomato robotic harvesting. IFAC-PapersOnLine, 2016; 49(16): 190–193.

[11] Wang X, Wu P, Feng Q, Wang G. Design and test of tomatoes harvesting robot. Journal of Agricultural Mechanization Research, 2016; 38(4): 94–98. (in Chinese)

[12] Yaguchi H, Nagahama K, Hasegawa T, Inaba M. Development of an autonomous tomato harvesting robot with rotational plucking gripper. 2016 IEEE/RSJ International Conference on Intelligent Robots and Systems (IROS), 2016; pp.652–657.

[13] Chen Z, Yang M, Li Y, Yang L. Design and experiment of tomato picking end-effector based on non-destructive pneumatic clamping control. Transactions of the CSAE, 2021; 37(2): 27–35. (in Chinese)

[14] Stephen L, Everett C, Lopes M M, Christopher B. Stronger at depth: jamming grippers as deep sea sampling tools. Soft Robotics, 2017; 4(4): 305–316.

[15] Brown E, Rodenberg N. Universal robotic gripper based on the jamming of granular material. Proceedings of the National Academy of Sciences of the United States of America, 2010; 107(44): 18809–18814.

[16] John A, Hod L. The JamHand: dexterous manipulation with minimal actuation. Soft Robotics, 2017; 4(1): 70–80.

[17] Tomokazu T, Kikuchi S, Suzuki M, Aoyagi S. Vacuum gripper imitated octopus sucker-effect of liquid membrane for absorption. 2015 IEEE/RSJ International Conference on Intelligent Robots and Systems, 2015; pp.2929–2936.

[18] Song S, Sitti M. Soft grippers using micro-fibrillar adhesives for transfer printing. Advanced Materials, 2014; 26(28): 4901–4906.

[19] Suresh S A, Christensen D L, Hawkes E W, Cutkosky M. Surface and shape deposition manufacturing for the fabrication of a curved surface gripper. Journal of Mechanisms and Robotics, 2015; 7(2): 1–7.

[20] Glick P, Suresh S A, Ruffatto III D, Cutkosky M, Tolley M T, Parness A. A soft robotic gripper with gecko-inspired adhesive. IEEE Robotics and Automation Letters, 2018; 3(2): 903–910.

[21] Wilson M. Festo drives automation forwards. Assembly Automation, 2011; 31(1): 12–16.

[22] Crooks W, Rozen-Levy S, Trimmer B, Rogers C, Messner W. Passive gripper inspired by Manduca sexta and the Fin Ray effect. International Journal of Advanced Robotic Systems, 2017; 14(4): 1–7.

[23] Crooks W, Vukasin G, O'Sullivan M, Messner W, Rogers C. Fin ray effect inspired soft robotic gripper: from the robosoft grand challenge toward optimization. Frontiers in Robotics and AI, 2016; 3: 70. doi: 10.3389/frobt.2016.00070.

[24] Hemming J, van Tuijl B A J, Gauchel W, Wais E. Field test of different end-effectors for robotic harvesting of sweet-pepper. Acta Horticulturae, 2016; 1130: 567–574.

[25] Hemming J, Bac W C, van Tuijl B A J, Barth R, Bontsema J, Pekkeriet E, et al. A robot for harvesting sweet-pepper in greenhouses. International Conference of Agricultural Engineering, Zurich, July 6-10, 2014; pp.1-8. Paper No. C0114.

[26] Preter A D, Anthonis J, Baerdemaeker J D. Development of a robot for harvesting strawberries. ScienceDirect, 2018; 51(17): 14–19.

[27] Shintake J, Cacucciolo V, Floreano D, Shea H. Soft robotic grippers. Advanced Materials, 2018; 30(29): 1707035. doi: 10.1002/adma.201707035.

[28] Chen Y, Guo S, Li C, Yang H, Hao L. Size recognition and adaptive grasping using an integration of actuating and sensing soft pneumatic gripper. Robotics and Autonomous Systems, 2018; 104: 14–24.

[29] Lu W, Wang P, Wang L, Deng Y. Design and experiment of flexible gripper for mushroom non-destructive picking. Transactions of the CSAM, 2020; 51(11): 28–36. (in Chinese)

[30] Li Z, Liu J, Li P. Relationship between mechanical property and damage of tomato during robot harvesting. Transactions of the CSAE, 2010; 26(5): 112–116. (in Chinese)

[31] Al-Rubaiai M, Pinto T, Qian C, Tan X. Soft actuators with stiffness and shape modulation using 3D-printed conductive polylactic acid material. Soft Robotics, 2019; 6(3): 1–15.